Int. J. Electrochem. Sci., 17 **(2022)** Article Number: 221229, doi: 10.20964/2022.12.39

International Journal of
ELECTROCHEMICAL
SCIENCE
www.electrochemsci.org

Nitrogen and Fluorine Codoped Graphite Derived from Microcrystalline Graphite ore as a High-performance Anode Material for Potassium-Ion Batteries

Guang Zhao[1], Jian Li[1], Linan Yang[2,], Zhikai Li[3], Yong Li[4], Yun Zhao[5,6,*]*

[1] Institute of New Materials for Chemical Energy Storage, Huayang New Material Science and Technology Group Co., Ltd., Yangquan 045000, PR China
[2] School of Chemistry and Chemical Engineering, Yangzhou University, Yangzhou 225002, PR China
[3] State Key Laboratory of Coal Conversion, Institute of Coal Chemistry, Chinese Academy of Sciences, Taiyuan 030001, PR China
[4] Research Center for Fine Chemicals Engineering, Shanxi University, Taiyuan 030006, PR China
[5] Institute of Molecular Science, Key Laboratory of Materials for Energy Conversion and Storage of Shanxi Province, Shanxi University, Taiyuan 030006, PR China
[6] Shanxi-Zheda Institute of Advanced Materials and Chemical Engineering, Taiyuan 030006, PR China
[*]E-mail: zhaoyun@sxu.edu.cn (Y. Zhao), yanglinan1996@163.com (L.N. Yang).

Received: 23 July 2022 / *Accepted:* 26 October 2022 / *Published:* 30 November 2022

Graphite, as a promising anode material for potassium-ion batteries (KIBs) suffers from poor cycling stability and rate performance. In this study, a nitrogen and fluorine codoping strategy was introduced to address these spiny issues. To investigate the practical effect, N,F-codoped graphite (NFMG) was prepared by means of a facile hydrothermal method with natural microcrystalline graphite (MG) ore and $(C_2H_5)_3N{\bullet}3HF$ solution as the raw materials. The results of material characterizations demonstrate that the hydrothermal treatment not only produces a prominent purification effect to remove the detrimental impurities of aluminosilicates, but also enlarges the interlayer spacing, decreases the crystal size and enriches the surface active sites of MG for K^+ association. Thus, the NFMG electrode exhibits a substantially elevated reversible capacity (335 mAh g^{-1}), favorable long-term cycling stability up to 500 cycles and excellent rate capability (96 mAh g^{-1} at 1.0 A g^{-1}). This study demonstrates the positive effect of heteroatom codoping on the K-storage performance of graphite for the first time and paves the way for the practical applications of high-performance KIBs.

Keywords: Heteroatom; Codoping; Graphite; Rate capability; Potassium-ion batteries.

1. INTRODUCTION

To make better use of intermittent green energy sources such as wind, waves and solar radiation, it is necessary to develop efficient and low-cost electric energy storage systems. Lithium-ion batteries (LIBs) with high energy density, long cycle life and mature technology are favored [1-3]. Unfortunately, the scarcity (0.0017%) of lithium resources (mainly in South America) and persistently high price of lithium salts make it difficult for LIBs to support the enormous market demands for large-scale energy storage. Therefore, many efforts have been made to search for suitable alternatives to LIBs. Among the potential candidates, potassium-ion batteries (KIBs) have drawn increasing attention because of the similar electrochemical working principle with LIBs and the high redox potential of K^+/K (-2.93 V vs. SHE) close to that of Li^+/Li (-3.04 V vs. SHE), which means a high energy density and operation voltage of KIBs [4,5].

Graphite, as a commercial anode material in LIBs, has a high theoretical specific capacity of 279 mAh g^{-1} when used in KIBs by forming a binary graphite intercalation compound of KC_8. However, the large radius of K^+ (1.38 Å) results in a large C-axis volume expansion of more than 60% during the potassiation reaction in the graphite host and sluggish reaction kinetics [6]. As a result, graphite materials always exhibit poor cycling life and rate performance, which hinders their practical applications. To address the issues of graphite anodes, the modification strategy for material structure mainly focuses on tuning the spacing between graphene layers and surface engineering by heteroatom doping or the introduction of defects [7,8]. For the regulation of graphite interlayer spacing, Liu's group [9] attempted to use the KOH activation method to prepare activated graphite. The enlarged interlayer distance and increased surface defects contribute to improved cycling stability and a high reversible capacity of 100 mAh g^{-1} at a current density of 0.2 A g^{-1} after 100 cycles. Feng [10] and Zhai's [11] teams used commercial expanded graphite and mildly expanded graphite as anode materials for KIBs, respectively. The expanded graphite shows a high reversible capacity of 263 mAh g^{-1} at 0.01 A g^{-1} and stable performance even after 500 discharge/charge cycles at 0.2 A g^{-1}, which is attributed to its enlarged interlayer spacing of 0.387 nm. For the preparation of mildly expanded graphite, a larger interplanar distance of 0.349 nm and a smaller grain size of 13 nm are realized by optimizing the ratio between the oxidation agent ($KMnO_4$) and intercalation agent (H_2SO_4). The optimized mildly expanded graphite exhibited a high capacity retention of 72.3% after 200 cycles at 0.1 A g^{-1}. Moreover, the rate capability was greatly enhanced. A high discharge capacity of 88 mAh g^{-1} can still be retained at the large current density of 1.5 A g^{-1}, indicating accelerated K^+ diffusion kinetics.

Surface heteroatom (e.g., N, S, F and P) doping into a graphitic framework is also an effective route to improve the performance of graphite materials by producing efficient defects, enhancing conductivity and enlarging the interplanar spacing of graphite layers [12-14]. In our previous work, the positive effect of F-doping on the potassium storage performance of microcrystalline graphite (MG) was proved [15]. Due to the introduction of highly electronegative F atoms, the graphite interlayer spacing was increased to 0.346 nm, and new surface active sites were created. The F-doped MG can maintain a stable reversible capacity of 238 mAh g^{-1} at 0.1 A g^{-1} with a high capacity retention of 74.6% after 100 cycles. Even though the rate performance is also elevated, it still needs to be further improved to cater to the fast-charging demand for practical applications. Binary or ternary heteroatom doping could be a

feasible avenue to further improve the K-storage performance of graphite materials. The favorable synergistic effect among the different doping atoms in carbonaceous hosts has been demonstrated in LIB and sodium-ion battery applications. Successful cases such as F,N-codoped graphene [16], S,N-codoped carbon nanotubes [17] and N,P-codoped soft carbon [18] have inspired the exploration of binary heteroatom doping for the development of high-performance graphite in KIBs. Herein, we investigate the effect of N,F codoping on the microstructure and K-storage performance of graphite for the first time. By employing MG ore and $(C_2H_5)_3N$•3HF as the starting materials, a N,F-codoped MG material (NFMG) was fabricated via a facile hydrothermal method, by which the purification of low-grade MG ore and N,F codoping were realized simultaneously. Benefiting from the synergistic effect of dual-heteroatom doping, a more defective surface texture was formed, and the graphite interlayer distance of the (002) plane was enlarged from 0.336 nm to 0.347 nm. The featured structural characteristics endow the NFMG electrode with a high reversible capacity of 244 mAh g^{-1} after 200 stable cycles at 0.1 A g^{-1} and substantially enhanced rate performance. A high discharge capacity of 96 mAh g^{-1} was achieved at a large current density of 1.0 A g^{-1}, which is 87.4% higher than that of fluorine-doped MG alone. The prominently improved cycling stability and rate capability of the NFMG electrode further prove the feasibility of multiple heteroatom doping for enhancing the K-storage performance of graphite material and pave the way to develop high-performance and practical KIBs.

2. EXPERIMENTAL

2.1. Preparation of the NFMG composite.

First, low-grade MG ore blocks (71 wt.%, Peking Jinglongte Carbon and Graphite Co., Ltd.) were crushed and screened to obtain MG powder with a particle size lower than 200 mesh. 65 wt.% trimethylamine tri-hydrofluoride ($(C_2H_5)_3N$•3HF, Aladdin, AR grade) solution was employed as the nitrogen and fluorine source. Next, 100 mg of MG powder was added to 30 mL of the $(C_2H_5)_3N$•3HF solution, and magnetically stirred for 1 h to realize a uniform dispersion. After that, the suspension liquid was transferred into a Teflon-lined autoclave (50 mL) and heat-treated at 150 ^oC for 10 hours with a rising rate of 5 ^oC min^{-1}. Finally, the as-obtained sediment was rinsed with deionized water until neutral and baked at 60 °C for 12 hours to obtain the resulting product.

2.2. Material characterization

The crystal structure of the samples was measured using X-ray diffraction (XRD) (Bruker D8 Advance using Cu Ka radiation at 40 kV, 40 mA). Raman spectra were tested by a Renishaw RM2000 spectroscopic system at an excitation line of 514 nm. The surface characteristics and bonding state of the samples were investigated by X-ray photoelectron spectroscopy (XPS) (Thermo ESCALAB250). The morphology and texture of the samples were observed by scanning electron microscopy (SEM, JIOL, JSM-7001F, 15 kV) and transmission electron microscopy (TEM, JEM 2010, JEOL, 200 kV) with energy dispersive spectrometry (EDS).

2.3. Electrochemical measurements

To prepare the working electrodes, 80% of the NFMG material, 10% acetylene black (conductive agent) and 10% polyvinylidene fluoride (adhesive agent) were dispersed in N-methylpyrrolidone and then ground in an agate mortar to form a uniform slurry. Subsequently, the slurry was coated on Cu foil and dried in a vacuum oven at 120 ^{o}C for 12 hours. The CR2025 coin half-cells were assembled in a glove box with a content of H_2O and O_2 <0.3 ppm. Potassium metal foils and glass microfiber membranes (Whatman) were served as the counter/reference electrodes and the separators, respectively. KPF_6 (0.8 M) in ethylene carbonate/diethyl carbonate (1:1 vol %) was used as electrolyte. The galvanostatic discharge/charge tests were tested within a voltage range of 0.01-3 V (vs K^+/K) using a multichannel battery test system (CT2001A, LAND, Wuhan). Cyclic voltammetry (CV) and electrochemical impedance spectroscopy (EIS) measurements were performed on a CHI 660E electrochemical workstation (Shanghai Chenhua). The scan rate of the CV test was 0.25 mV s^{-1}. The frequency of the EIS tests ranged from 100 kHz to 10 mHz and the voltage amplitude was 5 mV.

3. RESULTS AND DISCUSSION

3.1 Microstructure investigation of the NFMG material.

XRD patterns of the NFMG and the pristine MG are shown in Fig. 1a. For the pristine MG, addition to the characteristic (002) diffraction of graphite, many trivial impurity peaks are also discovered, which can mainly be indexed to quartz and aluminosilicates. In our previous work [15], we demonstrated that hydrofluoric acid leaching is a very effective method to purify MG ore, where a high purity of 98.59% is achieved. In the present study, $(C_2H_5)_3N•3HF$ is chosen as both the fluorine source and nitrogen source, and plays the role of purifying the MG ore powder. As seen in the XRD pattern of the NFMG, all of the impurity signals disappear completely after the hydrothermal process, and the (100), (101), (004) and (110) crystalline planes of graphite (JCPDS No. 41-1487) are exposed to the surface due to the removal of impurities. It is also noted that the (002) peak becomes much smaller and shifts distinctly left, indicating increased defects in the regular hexangular lattice structure and enlarged interlayer spacing. By calculating with Bragg's formula ($2d \sin\theta = n\lambda$) [19] and Scherrer's equation ($L_c = \frac{k\lambda}{\beta \cos\theta}$)[20], the interlayer distance of the 002 plane (d_{002}) and crystalline size (L_c) for the NFMG are 0.347 nm and 18.35 nm, respectively. Correspondingly, the values for the pristine MG are 0.336 nm and 26.83 nm, respectively. The enlarged d_{002} and decreased L_c are very beneficial to enhance the K^+ diffusion kinetics and alleviate volume fluctuation in NFMG during the potassiation/depotassiation process.

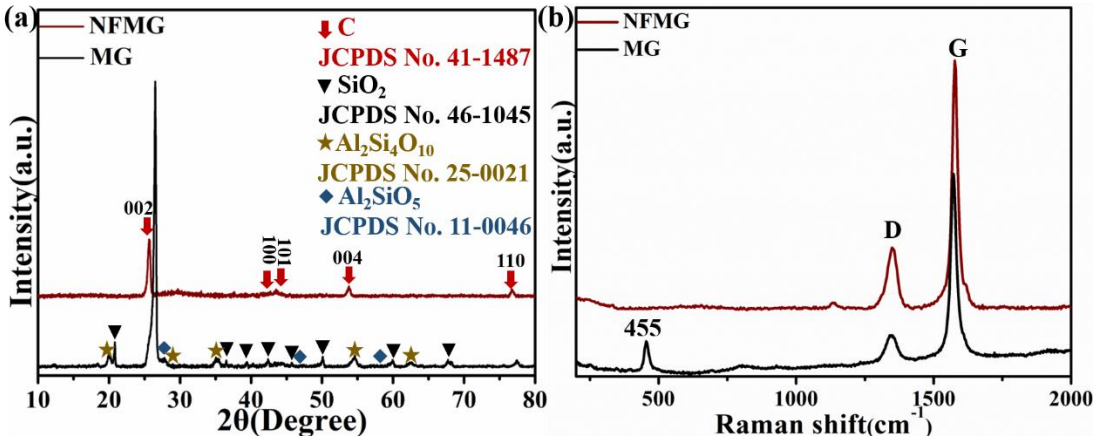

Figure 1. (a) XRD patterns and (b) Raman spectra of the NFMG and MG.

Raman spectra were further conducted to investigate the carbon structure variation after N and F codoping (Fig. 1b). There are two characteristic bands for graphite materials. The so-called D band located at approximately 1360 cm^{-1} represents amorphous carbon and defect structures in graphite lattices, and the G band located at approximately 1580 cm^{-1} is assigned to ordered sp^2 carbon arrangement structures [21]. The intensity ratio between the D band and G band (I_D/I_G) is inversely proportional to the graphitization degree of carbon materials. After a calculation, the I_D/I_G values for the NFMG and the pristine MG are 0.25 and 0.34, respectively. The lower I_D/I_G value of the NFMG could result from the removal of amorphous carbon and some unstable defects especially the surface oxygen functional groups, due to the hydrofluoric acid leaching treatment under hydrothermal conditions. In addition, the band at 455 cm^{-1} in the spectrum of MG is ascribed to the existence of aluminosilicates [22].

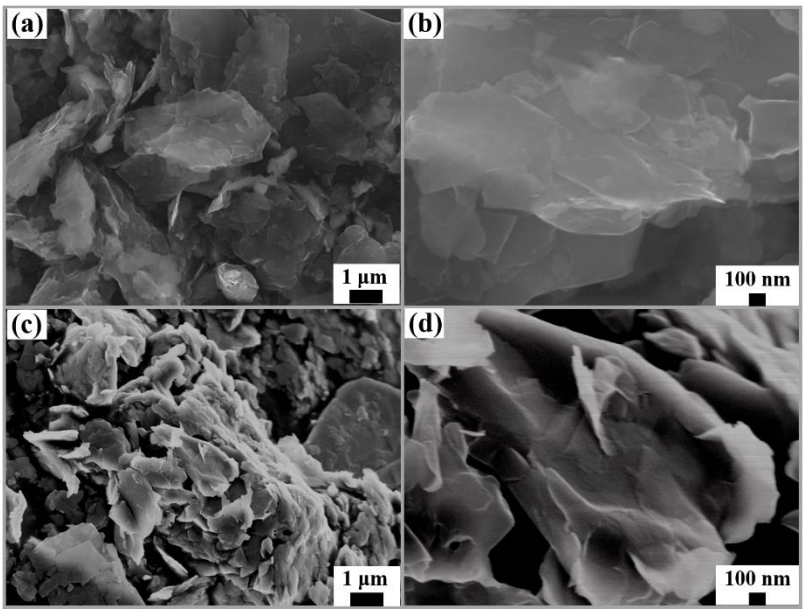

Figure 2. (a,b) SEM micrographs of MG. (c,d) SEM images with different magnifications for NFMG.

The morphologies of the NFMG and MG were characterized by SEM. As shown in Fig. 2a, the MG sample displays a typical laminar characteristic of graphite, where mingled impurity particles can be clearly observed. Fig. 2b shows that the large graphene layers pile up in an orderly manner to form a rough surface feature. After the hydrothermal process (Fig. 2c), one can see that the particle size of the NFMG decreases due to impurity removal and the etching effect of the agent $(C_2H_5)_3N•3HF$ on graphite lattices. Moreover, the elimination of impurities and amorphous carbon makes the surface of the NFMG loose and porous, which is favorable for convenient electrolyte permeation and K^+ diffusion. The carbon texture is further disclosed by TEM observation. As shown in Fig. 3a, the loose laminar structure in the NFMG consists of many irregular flakelets. The serrated edge and residual graphite domains on the surface of the graphite plane (Fig. 3b) are evidence of distinct etching during the hydrothermal reaction process. In addition, the lattice fringe of 0.208 nm corresponds to the (101) crystalline plane of graphite (JCPDS No. 41-1487). The elemental distribution in the NFMG was determined by TEM elemental mapping. As displayed in Fig. 3c-3g, the C, O, F and N elements are uniformly dispersed on the surface of the graphite plane, indicating the favorable homogeneity of the NFMG configuration.

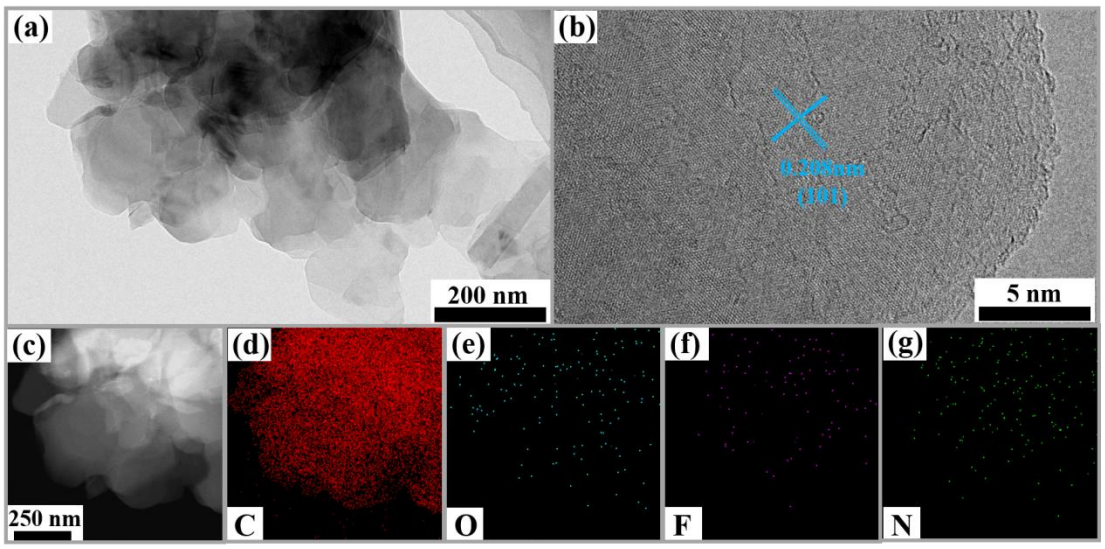

Figure 3. (a) TEM images and (b) HRTEM images of NFMG. (c) The dark-field TEM image of NFMG, and corresponding EDS mapping of C (d), O (e), F (f) and N (g).

The surface elements and chemical bonding state of the samples were investigated by XPS analyses. Fig. 4a shows the survey spectra of the NFMG and MG materials. In the spectrum of pristine MG, in addition to the obvious C and O peaks, several tiny peaks belonging to impurities can also be detected. Compared to that in MG, the impurity peaks vanish totally, accompanying the increased intensity of the C 1s peak and much weakened O 1s peak, indicating a favorable purification effect. It is noted that the F and N signals are inconspicuous in the NFMG spectrum, which could be due to the low content of F and N doping. The deconvoluted F 1s spectrum is shown in Fig. 4b. The peaks at 686.8 eV and 688.9 eV are attributed to semi-ionic C-F bonds and covalent C-F bonds, respectively [23]. The

existence of semi-ionic bonds in F-doping is beneficial to facilitate charge transfer and K^+ migration and contributes to improved rate performance. For the high-resolution N 1s spectrum, two N-doping types can be recognized, which include pyrrolic N at 400.2 eV and graphitic N at 401.3 eV [24]. According to previous reports [25,26], the existence of pyrrolic N produces abundant defects and adsorption active sites for K^+, while graphitic N can enhance the electronic conductivity and electrochemical reversibility of carbon materials. These positive effects would also be helpful to elevate the performances of the NFMG in some degree.

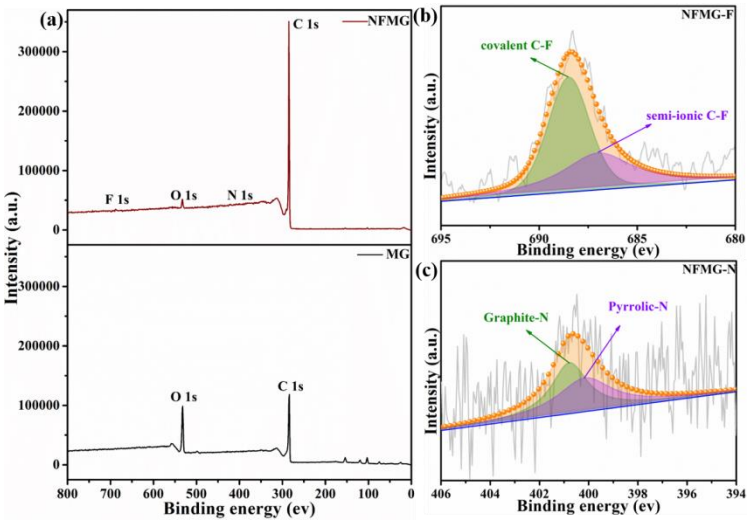

Figure 4. (a) XPS survey spectra of the NFMG and MG. (b) High-resolution F 1s spectrum and (c) N 1s spectrum of NFMG, respectively.

3.2. Electrochemical performance analyses of the NFMG.

To evaluate the effect of N and F codoping on the K-storage performance, the NFMG and the pristine MG electrode materials are assembled in 2025 coin-type half-cells and the performance comparison is carried out. Fig. 5a and 5b show the CV curves of the two electrodes, both of which show similar profiles, indicating an analogous redox reaction process. The irreversible reduction peak with a wide range of 0.2-1.1 V in the first cycle is ascribed to electrolyte decomposition and the formation of a solid-electrolyte interface layer on the surface of the electrode material [27]. The sharp reduction peak at 0.01 V and the distinct oxidation peak at approximately 0.35 V are related to the insertion and extraction of K^+ on the graphite host, respectively [28]. The pair of reduction/oxidation peaks overlapped well after the first cycle, indicating the good reversibility of the redox reaction. It is noted that the anodic peaks in the NFMG are narrower and higher than those in the pristine MG, suggesting the better reaction activity of the K^+ extraction from graphite layers due to the improved electrode structure. The galvanostatic discharge-charge curves present electrochemical behaviors consistent with those in the CV analyses. The multiplateaus characteristic in the discharge profiles reflect the stepwise intercalation process of K^+ into the graphite layers from KC_{60} to the final stable product of KC_8. Based on the

insertion/deinsertion reaction mechanism, the NFMG electrode releases discharge/charge capacities of 836/335 mAh g^{-1} in the first cycle with an initial Coulombic efficiency of 40.1%. In contrast, the corresponding values for the pristine MG are 552/181 mAh g^{-1} and 32.8%, respectively. The much elevated reversible capacity and initial Coulombic efficiency demonstrate the prominent modification effect of N,F-codoping and impurity removal, which diminishes the undesired side reactions at the electrolyte/electrode interface and increases the reactivity of the host material.

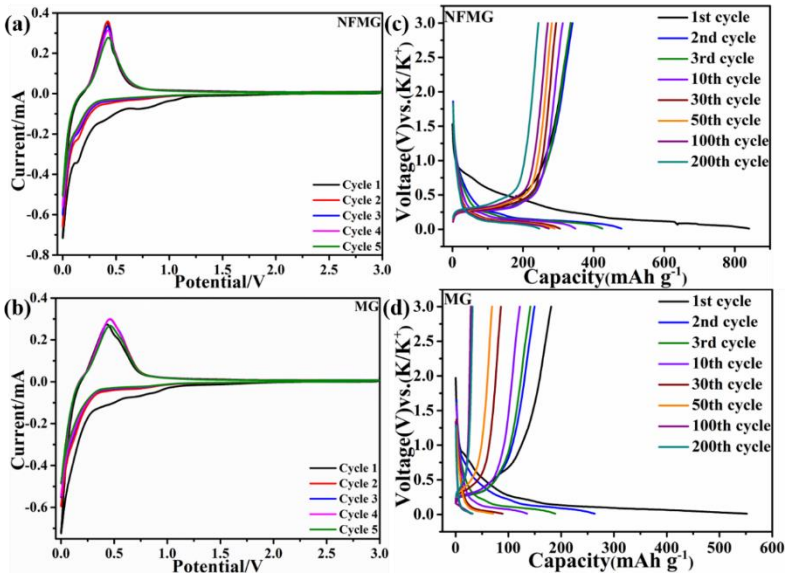

Figure 5. (a,b) CV curves of NFMG and MG electrodes. (c,d) Galvanostatic discharge/charge profiles at various cycles of the NFMG and MG electrodes at a current density of 0.1 A g^{-1}.

The cycling performance comparison between the NFMG and the pristine MG is displayed in Fig. 6a. Both electrodes show some capacity decay in the initial several cycles due to the potassiation-induced structural rearrangement. As shown in Fig. 5c and 5d, the decay extent of the NFMG is much weaker than that of the MG, indicating better electrode structure stability. After the initial 20 cycles, the reversible capacity gradually remains stable, and a high discharge capacity of 252 mAh g^{-1} at 0.1 A g^{-1} can be well maintained. In sharp contrast, the pristine MG presents rapid capacity decay with cycling. A poor discharge capacity of only 31 mAh g^{-1} remains after 100 cycles because of its inferior structural stability. The rate capability of the NFMG is also greatly improved. As shown in Fig. 6b, with the stepwise raised current densities from 0.1, 0.2, 0.4, 0.6, 0.8 and 1.0 A g^{-1}, reversible capacities of 305, 292, 242, 201, 139 and 96 mAh g^{-1} are obtained, respectively, while the corresponding values for pristine MG are much inferior at the same current densities. Moreover, when the current density is reset to 0.1 A g^{-1}, a high reversible capacity of 297 mAh g^{-1} is immediately restored and remains stable in the following cycles, manifesting the excellent rate ability and structural stability. To further evaluate the potential of the NFMG in long-life KIBs, a long-term cycling test is carried out. From the result shown in Fig. 6c, the NFMG electrode exhibits a satisfactory capacity stability with cycling. Even after 500 discharge/charge cycles at 0.4 A g^{-1}, a high discharge capacity of 163 mAh g^{-1} can still be retained with

a low capacity loss of 0.065% per cycle. The superior electrochemical performance is also compared with the recently reported graphite electrode materials in KIB applications (Table 1). It can be seen that the NFMG presents a higher reversible capacity, favorable cycling stability and better rate ability, demonstrating its advantages in the current level of graphite for the performance of K-storage.

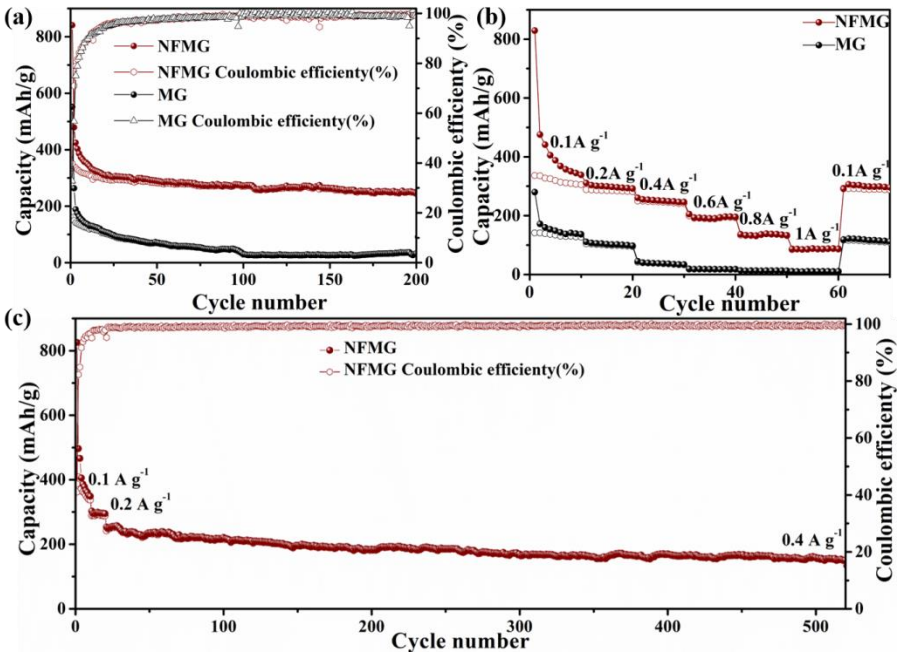

Figure 6. (a) Cycling performances of NFMG and MG electrodes at 0.1 A g^{-1} for 200 cycles. (b) Rate capabilities of NFMG and MG electrodes at various current densities. (c) Long-term cyclability of NFMG electrode at 0.4 A g^{-1} for 500 cycles.

The substantially improved electrochemical performance of the NFMG is attributed to the following two reasons. On the one hand, the removal of impurities by the hydrothermal reactions diminishes the irreversible side reactions of the electrode material with electrolyte, and meanwhile increases the relative content of active matter, which contributes to the higher initial Coulombic efficiency and specific capacity of NFMG than pristine MG. On the other hand, the synergistic effect of fluorine and nitrogen codoping not only enlarges the interlayer spacing of MG to alleviate the C-axis volume expansion and facilitate K^+ diffusion, but also enriches the surface active sites for K^+ association and elevates the conductivity for faster charge transfer, resulting in greatly enhanced cycling stability and rate performance.

Table 1. Comparison of the electrochemical performance among the NFMG and the modified graphite reported in references.

Graphite materials	Cycle performance			Rate performance	
	Current density (A g^{-1})	Capacity after 100 cycles (mAh g^{-1})	Capacity retention after 100 cycles (%)	Current density (A g^{-1})	Discharge capacity (mAh g^{-1})
NFMG (This work)	0.1	270	80.6	0.6	193
F-doped graphite [15]	0.1	238	74.6	0.6	126
Mildly-expanded graphite [11]	0.1	195	88.1	0.6	135
Expanded graphite [10]	0.05	228	81.5	0.2	175
Activated MG [29]	0.1	186	71.0	0.6	162
Activated graphite [7]	0.2	100	31.5	0.4	114
F-doped carbon-coated graphite [30]	0.1	178	70.9	0.6	142
Ball-milled graphite [31]	0.025	162	65.0	0.25	180

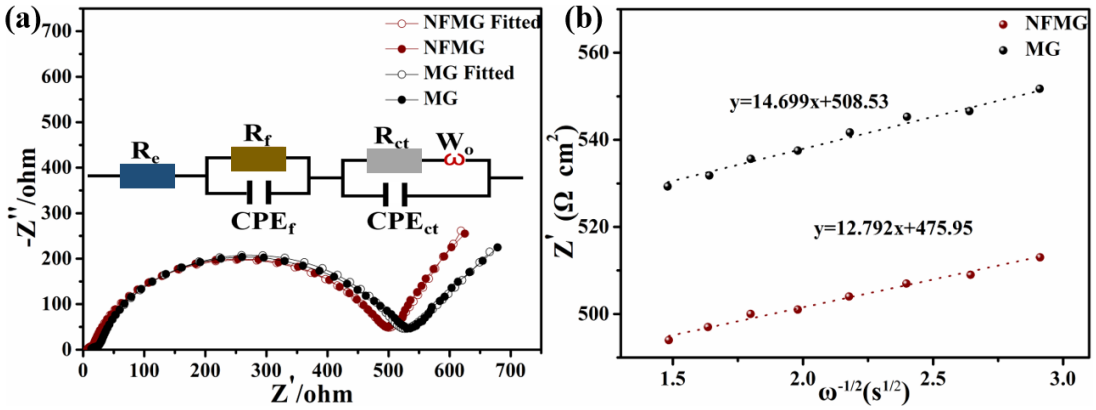

Figure 7. (a) Nyquist plots of the NFMG and MG electrodes after 3 cycles at 0.1 A g^{-1}. The inset is the equivalent circuit used for fitting. (b) The relationship between Z' and $\omega^{-1/2}$.

The enhanced K^+/e^- transformation kinetics is further demonstrated by EIS analyses. Fig. 7a displays the Nyquist plots of the NFMG and MG electrodes. Both electrodes manifest a semicircle in the high to mediate-frequency region and an inclined line in the low-frequency region, which is related to charge transfer and K^+ diffusion in the electrode material, respectively [32]. After value fitting by the

equivalent circuit shown in the inset of Fig. 7a, it is found that the value of R_{ct} (458 Ω) for the NFMG is smaller than that for the pristine MG (472 Ω), suggesting the higher electric conductivity of the NFMG electrode. In addition, the K^+ diffusion ability is inversely proportional to the Warburg factor (σ). σ is related to the relationship [33]: $Z' = R_D + R_L + \sigma\omega^{-1/2}$ and can be obtained by calculating the slope of the inclined line shown in Fig. 7b. The smaller value (12.79) of σ for the NFMG electrode compared with that (14.70) for the MG electrode signifies the faster K^+ diffusion kinetics, and thereby the rate capability of the NFMG electrode is significantly enhanced.

4. CONCLUSION

In summary, a fluorine and nitrogen codoping strategy has been developed to address the issues of graphite when used as anode material for KIBs. Microcrystalline graphite (MG) ore powder was employed as the prototype to fabricate N,F-codoped graphite (NFMG) through a facile hydrothermal route in $(C_2H_5)_3N$•3HF solution. The results manifest that impurity removal and N,F-codoping are simultaneously achieved. The codoping plays a favorable synergistic effect to modify the graphite structure, especially contributing to the enlarged interlayer spacing of 0.346 nm and decreased crystalline size of 18.35 nm. As a result, the NFMG electrode exhibits substantially elevated reversible capacity, improved cycling stability and excellent rate capability. These results demonstrate that heteroatom codoping is a feasible avenue to develop high-performance graphite materials for KIBs.

ACKNOWLEDGEMENTS
This work was financially supported by the research project from Shanxi-Zheda Institute of Advanced Materials and Chemical Engineering [No. 2022SX-TD028] and National Natural Science Foundation of China [No. 51702191].

References

1. A. hajizadeh, T. Shahalizade, R. Riahifar, M.S. Yaghmaee, B. Raissi, S. Gholam, A. Aghaei, S. Rahimisheikh, A.S. Ghazvini, *J. Power Sources,* 535 (2022) 231448.
2. S.Q. Zhang, Q.F. Zhao, C. Wang, M.Y. Hu, J.H. Ge, X.N. Yu, G.H. Jiang, Q.S. Ouyang, *Int. J. Electrochem. Sci.,* 17 (2022) 220237.
3. L. Wang, L. Ren, Y. Qin, J. Chen, H. Chen, K. Wang, H. Liu, Z. Huang, Q. Li, *Int. J. Electrochem. Sci.,* 17 (2022) 220221.
4. N. Khan, G.H. Han, S. A. Mazari, *J. Electroanal. Chem.,* 907 (2022) 116051.
5. K. Zhang, Z. Gu, E.H. Ang, J. Guo, X. Wang, Y.L. Wang, X. Wu, *Mater. Today,* 54 (2022) 189.
6. Y. Lei, J.L. Wang, D. Han, F. Yuan, H.W. Wang, R.Y. Zhao, D.Q. Huang, Y.Y. Wu, B. Zhang, D.Y. Zhai, F.Y. Kang, *Carbon,* 196 (2022) 229.
7. J.T. Xu, Y.H. Dou, Z.X. Wei, J.M. Ma, Y.H. Deng, Y.T. Li, H.K. Liu, S.X. Dou, *Adv. Sci.,* 4 (2017) 1700146.
8. C.Y. Meng, M. Yuan, B. Cao, X.J. Lin, J.P. Zhang, A. Li, X.H. Cheng, M.Q. Jia, H.H. Song, *Carbon,* 192 (2022) 347.
9. Z.X. Tai, Q. Zhang, Y.J. Liu, H.K. Liu, S.X. Dou, *Carbon,* 123 (2017) 54-61.
10. Y.L. An, H.F. Fei, G.F. Zeng, L.J. Ci, B.J. Xi, S.L. Xiong, J.K. Feng, *J. Power Sources,* 378 (2018) 66.

11. X.J. Li, Y. Lei, L. Qin, D. Han, H.W. Wang, D.Y. Zhai, B.H. Li, F.Y. Kang, *Carbon,* 172 (2021) 200.
12. B. Wang, L. Gu, F. Yuan, D. Zhang, H.L. Sun, J. Wang, Q.J. Wang, H. Wang, Z.J. Li, *Chem. Eng. J.,* 432 (2022) 134321.
13. T. Jeon, S. Lee, S.C. Jung, *Curr. Appl Phys.,* 20 (2020) 988.
14. J.S. Park, D.Y. Park, S.M. Yang, J.H. Ryu, J.H. Park, S.M. Kim, H. Jin, C.R. Park, J.H. Kim, S.J. Yang, *Carbon,* 196 (2022) 304.
15. Y. Zhao, L.N. Yang, C.L. Ma, G.Y. Han, *Energy Fuels,* 34 (2020) 8993.
16. H.R An, Y. Li, Y. Gao, C. Cao, J.K. Han, Y.Y. Feng, W. Feng, *Carbon,* 116 (2017) 338.
17. Y.C. Li, R. Mi, S.M. Li, X.C. Liu, W. Ren, H. Liu, J. Mei, W. Lau, *Int. J. Hydrogen Energy,* 39 (2014) 16073.
18. X.Q. Ma, N. Xiao, J. Xiao, X.D. Song, H.D. Guo, Y.T. Wang, S.J. Zhao, Y.P. Zhong, J.S. Qiu, *Carbon,* 179 (2021) 33-41.
19. Z. Li, C. Lu, Z. Xia, Y. Zhou, Z. Luo, *Carbon,* 45 (2007) 1686.
20. Z. Ju, S. Zhang, Z. Xing, Q. Zhuang, Y. Qiang, Y. Qian, *ACS Appl. Mater. Interfaces,* 8 (2016) 20682.
21. A.P. Vijaya Kumar Saroja, M. Muruganathan, K. Muthusamy, H. Mizuta, R. Sundara, *Nano Lett.,* 18 (2018) 5688.
22. T.K. bechgaard, G. Scannell, L. Huang, R.E. Youngman, J.C. Mauro, M.M. Smedskjaer, *J. Non-Cryst. Solids,* 470 (2017) 145.
23. S. Huang, Y. Li, Y. Feng, H. An, P. Long, C. Qin, W. Feng, *J. Mater. Chem.* A, 3 (2015) 23095.
24. H.H. Wang, G. Yang, Z. Chen, J.L. Liu, X.F. Fan, P. Liang, Y.Z. Huang, J.Y. Lin, Z.X. Shen, *J. Power Sources,* 419 (2019) 82-90.
25. Y.H. Xie, Y. Chen, L. Liu, P. Tao, M.P. Fan, N. Xu, X.W. Shen, C.L. Yan, *Adv. Mater.,* 29 (2017) 1702268.
26. J.L. Yang, Z.C. Ju, Y. Jiang, Z. Xing, B.J. Xi, J.K. Feng, S.L. Xiong, *Adv. Mater.,* 30 (2018) 1700104.
27. L.P. Wang, J.Y. Yang, J. Li, T. Chen, S.L. Chen, Z.R. Wu, J.L. Qiu, B.J. Wang, P. Gao, X.B. Niu, H. Li, *J. Power Sources,* 409 (2019) 24.
28. L. Fan, R. Ma, Q. Zhang, X. Jia, B. Lu, *Angew. Chem. Int. Ed.,* 58 (2019) 10500.
29. L.N. Yang, Y. Zhao, C.L. Ma, G.Y. Han, *J. Mater. Sci.- Mater. Electron.,* 32 (2021) 24446.
30. L.N. Yang, Y. Zhao, L.J. Cao, H.L. Chen, G.Y. Han, *Energy Fuels,* 35 (2021) 5308.
31. M. Carboni, A.J. Naylor, M. Valvo, *RSC adv.,* 9 (2019) 21070.
32. Y.S. Wang, Q.C. Wang, X.Y. Ding, M. Wang, Y.H. Xin, *Appl. Surf. Sci.,* 601 (2022) 154218.
33. T. Jin, Y.C. Liu, Y. Li, K.Z. Cao, X. J. Wang, L.F. Jiao, *Adv. Energy Mater.,* 7 (2017) 1700087.